JNeurosci
THE JOURNAL OF NEUROSCIENCE

Research Articles: Development/Plasticity/Repair

Persistent Cyfip1 expression is required to maintain the adult subventricular zone neurogenic niche

https://doi.org/10.1523/JNEUROSCI.2249-19.2020

Cite as: J. Neurosci 2020; 10.1523/JNEUROSCI.2249-19.2020

Received: 17 September 2019
Revised: 7 January 2020
Accepted: 21 January 2020

[JN-RM-2249-19]

Title: Persistent Cyfip1 expression is required to maintain the adult subventricular zone neurogenic niche

Abbreviated Title: Cyfip1 in the adult neurogenic niche

Christa Whelan Habela[1], Ki-Jun Yoon[1,3,4], Namshik Kim[1,4], Arens Taga[1], Kassidy Bell[1], Dwight E. Bergles[2], Nicholas J. Maragakis[1], Guo-li Ming[1,4,5,6,7] and Hongjun Song[1,4,5,6,8]

[1]Department of Neurology, [2]The Solomon H. Snyder Department of Neuroscience, Johns Hopkins University Baltimore, MD, 21287, USA.
[3]Korea Advanced Institute of Science and Technology, College of Life Science and Bioengineering, Department of Biological Sciences, Daejeon 34141, Republic of Korea.
[4]Department of Neuroscience and Mahoney Institute for Neurosciences, [5]Institute for Regenerative Medicine, [6]Department of Cell and Developmental Biology, [7]Department of Psychiatry, [8]The Epigenetics Institute, Perelman School of Medicine, Philadelphia, PA, 19104, USA.

Corresponding Author:
Hongjun Song, Ph.D.
Perelman School of Medicine at University of Pennsylvania, Department of Neuroscience, 415 Curie Blvd., Clinical Research Building Suite 111B, Philadelphia, PA 19104, USA.
Office: 215-573-2449
Email: shongjun@pennmedicine.upenn.edu

Co-Corresponding Author:
Christa Whelan Habela, M.D, Ph.D.
Johns Hopkins Medicine, Department of Neurology, 600 North Wolfe Street, Meyer 2-147, Baltimore, MD 21287, USA.
Email: chabela1@jhmi.edu

Number of pages: 30
Number of figures: 7
Number of words – Abstract: 226
Number of words – Introduction: 604
Number of words – Discussion: 1436

Conflict of interest: No conflicts to disclose.

Acknowledgements: This work was supported by grants from NIH (R25NS065729 and K12NS098482 to C.W.H., R37NS047344 to H.S., R35NS097370 to G-l.M), SFARI (308988 to H.S.), and DOD (W81XWH1810174 ALSRP to N.J.M.). The *Nestin-CreER* animals were kindly provided by Gordon Fishell. We are grateful to lab members of the Song and Ming laboratories for feedback and technical support, in particular Kim Christian, Daniel Berg, Allison Bond, Tong Ma, Yi Zhou, Fadi Jacob and Jordan Schnoll.

Author contributions: C.W.H. led the project, collected data and was involved in all aspects of the study. K-J.Y. and N.K. generated the *Cyfip1* floxed animals and planned breeding paradigms. K.B. assisted with immunostaining and animal breeding. A.T. contributed to data analysis. G-l.M., N.J.M. and D.E.B contributed to analysis, experimental design and writing. C.W.H., KJ-Y, G-l.M. and H.S. conceived of the project and experimental design. G-l.M. and H.S. oversaw the project. C.W.H. and H.S. wrote the manuscript.

[JN-RM-2249-19]

ABSTRACT

Neural stem cells (NSCs) persist throughout life in the subventricular zone (SVZ) neurogenic niche of the lateral ventricles as type B1 cells in adult mice. Maintaining this population of NSCs depends on the balance between quiescence and self-renewing or self-depleting cell divisions. Interactions between B1 cells and the surrounding niche are important in regulating this balance, but the mechanisms governing these processes have not been fully elucidated. The cytoplasmic FMRP-interacting protein (Cyfip1) regulates apical-basal polarity in the embryonic brain. Loss of Cyfip1 during embryonic development in mice disrupts the embryonic niche and affects cortical neurogenesis. However, a direct role for Cyfip1 in the regulation of adult NSCs has not been established. Here, we demonstrate that Cyfip1 expression is preferentially localized to B1 cells in the adult mouse SVZ. Loss of *Cyfip1* in the embryonic mouse brain results in altered adult SVZ architecture and expansion of the adult B1 cell population at the ventricular surface. Furthermore, acute deletion of *Cyfip1* in adult NSCs results in a rapid change in adherens junction proteins as well as increased proliferation and number of B1 cells at the ventricular surface. Together, these data indicate that Cyfip1 plays a critical role in the formation and maintenance of the adult SVZ niche and, furthermore, deletion of *Cyfip1* unleashes the capacity of adult B1 cells for symmetric renewal to increase the adult NSC pool.

SIGNIFICANCE: Neural stem cells (NSCs) persist in the subventricular zone (SVZ) of the lateral ventricles in adult mammals and the size of this population is determined by the balance between quiescence and self-depleting or renewing cell division. The mechanisms regulating these processes are not fully understood. This study establishes that the cytoplasmic FMRP interacting protein 1 (Cyfip1) regulates NSC fate decisions in the adult SVZ and adult NSCs that are quiescent or typically undergo self-depleting divisions retain the ability to self-renew. These results contribute to our understanding of how adult NSCs are regulated throughout life and has potential implications for human brain disorders.

INTRODUCTION

Neural stem cells (NSCs) persist in the subventricular zone (SVZ) of the lateral ventricles into adulthood in mammals (Doetsch et al., 1999; Bond et al., 2015; Altman, 1969). The adult SVZ recapitulates the developmental NSC niche with an apical-basal polarity of NSCs, referred to as type B1 cells (Lois and Alvarez-Buylla, 1993; Doetsch et al., 1999). The cell bodies of B1 cells lie beneath the ependymal cell layer and undergo symmetric self-renewing divisions to maintain their population or self-depleting divisions to generate olfactory bulb interneurons or oligodendrocyte precursors (Parras et al., 2004; Menn et al., 2006; Rousselot et al., 1995; Lois and Alvarez-Buylla, 1994; Lois and Alvarez-Buylla, 1993; Obernier et al., 2018). Disruption of the SVZ niche leads to alterations in B1 cell proliferation as well as neuronal and oligodendrocyte genesis (Kokovay et al., 2012; Jimenez et al., 2009; Relucio et al., 2012). The niche structure changes with age as B1 cells are depleted (Shook et al., 2012; Obernier et al., 2018), but the cellular mechanisms regulating niche maintenance and B1 cell fate in the adult brain have still not been fully elucidated.

Type B1 cells project apical processes to the ventricular surface and basal processes to the vasculature underlying the adult SVZ. At the ventricle, the apical processes are surrounded by ependymal cells forming an epithelial surface and oriented in a pinwheel-type formation around the apical processes (Mirzadeh et al., 2008; Alvarez-Buylla and Lim, 2004; Mercier et al., 2002; Doetsch et al., 1999). Central to the niche structure in both the embryo and adult is the maintenance of apical-basal polarity (Lian and Sheen, 2015; Bizzotto and Francis, 2015; O'Leary et al., 2017; Yoon et al., 2014). During embryonic development, radial glial cells (RGCs) make apical connections to the ventricular surface and basal projections to the pia and the orientation of the division plane along the apical-basal axis regulates the fate of daughter cells (Gotz and Huttner, 2005; Kosodo et al., 2004). This polarity is determined by the presence of adherens junctions and the loss of junction integrity during fetal development leads to alterations in cellular polarity and abnormal neural development (O'Leary et al., 2017; Bizzotto and Francis, 2015; Ferland et al., 2009; Guerra et al., 2015; Yoon et al., 2014; Lian and Sheen, 2015).

The stability of adherens junctions depends on cadherins interacting with the cytoplasmic actin ring (O'Leary et al., 2017; Priya and Yap, 2015; Verma et al., 2012). This process is mediated by Arp2/3-dependent actin nucleation and the WAVE regulatory complex (WRC) (Verma et al., 2012; Wang et al., 2016). Cytoplasmic FMRP interacting protein1 (Cyfip1) interacts with Rac-GTP to cleave the WRC, resulting in actin polymerization. Cyfip1 regulates apical-basal polarity and its loss during the embryonic development results in adherens junction deficits (Yoon et al., 2014). Adult *Cyfip1* haploinsufficient mice exhibit impaired myelination and a decreased number of oligodendrocytes in the corpus callosum as well as behavioral abnormalities (Silva, A. I., Haddon et al., 2019; Dominguez-Iturza et al., 2019).

In this study we show persistent expression of Cyfip1 in type B1 cells of the adult SVZ in mice with prominent localization to the apical processes projecting to the ventricular surface. Deletion of *Cyfip1* during embryonic development results in an expansion of the B1 cell population, as well as altered localization and increased proliferation rates in the adult SVZ. Acute loss of *Cyfip1* in the adult SVZ NSCs is sufficient to alter the localization and increase proliferation rates of B1 cells, suggesting that Cyfip1 suppresses symmetric B1 cell expansion in adult mice. Changes in adherens junction protein localization parallels decreases in Cyfip1 expression and supports an underlying loss of adherens junction stabilization.

MATERIALS AND METHODS

Animals

All transgenic animals were crossed on a C57/Bl6 background. The *Nestin-CreER* animals were kindly provided by Gordon Fishell (Balordi and Fishell, 2007). *Nestin-Cre* (JAX stock #003771: B6.Cg-Tg(Nes-cre)1Kln/J) (Giusti et al., 2014; Tronche et al., 1999) and *mTmG* reporter mice (Stock # 007676: B6.129(Cg)-Gt(ROSA)26Sortm4(ACTB-tdTomato,-EGFP)Luo/J) (Muzumdar et al., 2007) were obtained from the Jackson Laboratory (Bar Harbor, ME).

In order to generate a *Cyfip1* floxed allele (*Cyfip1*^{f}), a targeting vector was designed to insert a *loxP* sequence in front of exon 2 as well as a positive selection marker (PGK promoter driven neomycin resistant gene) together with another *loxP* sequence next to exon 5. This was constructed by recombineering as described (Liu et al., 2003). Specifically, an 11.9 kb genome fragment containing exon 2 to exon 5 from 129Sv BAC clone (bMQ182K14, Source Bioscience) was retrieved into a PL253 plasmid containing a negative selection marker (MC1 promoter driven thymidine kinase gene) using homologous recombination. A *loxP* sequence and an Flpe-PGK-EM7-Neo-Flpe-loxP cassette were sequentially inserted into the engineered PL253, resulting in 6.0 kb and 1.0 kb homology arms. The targeting vector was linearized and electroporated into 129S4/Sv Jae embryonic stem cells (The Transgenic Core Laboratory in Johns Hopkins School of Medicine), and homologous recombination was confirmed by PCR screening. Targeted clones were injected into C57BL/6J blastocysts, which were subsequently transferred into pseudo-pregnant foster mothers. Confirmation of germ-line transmission of the floxed allele and routine genotyping were performed by PCR screening on tail genomic DNA (wt, 470bp; floxed, 520bp) using DNA primers as follows: 5'-GCACCTCTCTGCATTTCTGT-3' and 5'-GCACCAATCAAGTGTTTTCC-3'.

For conditional knockout experiments, homozygous *Cyfip1*$^{f/f}$ animals were crossed with animals heterozygous for *Nestin-Cre to generate Nestin-Cre*:*Cyfip1*$^{f/f}$ males that were heterozygous for *Nestin-Cre* with homozygous floxed *Cyfip1* alleles. These were subsequently bred with *Cyfip1*$^{f/f}$ females resulting in 50% control (*Cyfp1*$^{f/f}$) and 50% conditional knockout (cKO) animals (*Nestin-Cre:Cyfip1*$^{f/f}$). Inducible breeding pairs were made up of *Nestin-CreER:Cyfip1*$^{+/f}$*:mTmG* males crossed with *Cyfip1*$^{+/f}$*:mTmG* females. The *mTmG* allele was either heterozygous or homozygous in experimental animals.

All experiments involving animals were approved by the animal care and use committee at Johns Hopkins University. Both male and female animals were used for experiments. Animals were housed under 14 hour light/10 hour dark housing conditions with standard diets and water *ad libitum*.

Immunohistochemistry

Anaesthetized animals were perfused with phosphate buffered saline (PBS) followed by 4% paraformaldehyde (PFA). Brains were removed from skulls and placed in 4% PFA overnight and no longer than 24 hours at 4°C. They were then washed one time with PBS and placed in a 30% sucrose in PBS at 4°C for a minimum of 48 hours prior to sectioning. Serial coronal brain sections were prepared using a sliding microtome (Leica, SM2010R) or a cryostat (ThermoFisherHM 505 and an HM 550) after brains were frozen in either 30% sucrose solution or OCT freeze solution (Sigma). Sections were stored frozen in multi-well plates containing antifreeze solution (300 g sucrose, 300 ml ethylene glycol, 500 ml 0.1 M PBS). Prior to antibody immunostaining, anti-freeze solution was removed and sections were washed 2 times with PBS. Antibody solutions were made up of 5% donkey or goat serum, 3% bovine serum albumin and 0.05% Triton X 100 in PBS or tris buffered saline. Primary antibodies were incubated at 4°C for 24 to 72 hours. Sections were washed 3 times in 0.05% Triton-X 100 in PBS solution prior to secondary antibody application. Secondary antibodies were diluted in the above-described antibody solution using goat Alexa Fluor 488, 555, 568, and 647 secondary antibodies (ThermoFisher Scientific) at 1:400 dilutions in antibody solution with 5% goat serum or donkey Cy2, CY3 and Cy5 antibodies (Jackson ImmunoResearch) at 1:250 dilution in antibody solution containing 5% donkey serum. Secondary antibody solutions were incubated either at room temperature for 2 to 4 hours or overnight at 4°C. Hoechst 33342 (Sigma) or DAPI (Roche) nuclear stains were added to the secondary antibody solutions. For antibodies that required antigen retrieval, brain sections were incubated in Dako 1X target retrieval solution (Agilent Dako) or sodium acetate buffer, pH 6 (Sigma) at 95°C for 20 minutes then room temperature for 20 minutes prior to staining. If green fluorescent protein (GFP) staining was required, anti-GFP primary and secondary antibody staining was conducted prior to the antigen retrieval step. Tissue was mounted on Superfrost™ or Superfrost Plus™ slides (Fisher) and coverslipped with 2.5% PVA/DABCO mounting media (Sigma) or ProLong Antifade mounting

media (ThermoFisher). Specific antibodies are noted in the results section and include: mouse anti-β-Catenin (BD Biosciences, Cat # 610153), mouse anti-ɣ-Tubulin (Abcam, Cat # ab11316), rabbit anti-GFAP (Dako, Cat # Z0334), rabbit anti-Cyfip1 (Millipore-Sigma, Cat # Ab6046), rabbit anti-β-Catenin (ThermoFisher, Cat # PA5-16762), chicken anti-GFP (Aves, Cat # NC9510598), mouse anti-N-Cadherin (Invitrogen, Cat # 981235A), rabbit anti-S100β (Sigma, Cat # HPA015768), mouse anti-S100β (Sigma, Cat # AMAB91038), goat anti-Sox2 (Santa Cruz Biotechnology, Cat # SC17320), rabbit anti-hASH1 (MASH1) (Cosmo Bio Co., Ltd., Cat # SK-T01-003), and rabbit anti-Doublecortin (Dcx) (Cell Signaling Technologies, Cat # 4604S).

Whole-mount Preparation

Whole-mount preparations of the ventricular wall were prepared using a protocol modified from that published by Mirzedah et al (Mirzadeh et al., 2010). The one modification made was that animals were perfused with 4% PFA prior to starting the dissection rather than afterwards. Immunostaining of the whole-mount sections was performed as described above.

Cell Proliferation Quantification

Cells undergoing DNA replication in S phase were identified by incorporation of 5-ethynyl-2'-deoxyuridine (EDU) (Sigma, St. Louis, MO. Cat # 900584). A stock concentration of 32.5 mM EDU was made by adding EDU to sterile saline solution with the addition of 1:1000 5 M NaOH and heating to 42°C for 30 to 60 minutes to dissolve. Stock solutions were stored at -80°C. Two to twenty four hours prior to perfusion, the solution was warmed to 37°C and intraperitoneal injections were conducted on 56-84 day old animals for a final dose of 200 mg/kg body weight. After perfusion and antibody staining, the standard commercial protocol for the Click-iT^{TM} Plus EDU cell proliferation kit for Imaging (ThermoFisher Scientific, Waltham, MA. Cat. # C10639) was used to fluorescently label the EDU incorporated into the newly synthesized DNA. Three-dimensional (3D) tiled images were obtained of the sections and images were reconstructed either in Imaris 3D

software (Bitplane), Image J Software (NIH) or ZEN software (Carl Zeiss Microscopy, Jena, Germany). EDU^+ cell numbers were manually quantified based on the presence of EDU fluorescence in the cell nuclei.

Tamoxifen Injection

A stock solution of 66.7 mg/mL of tamoxifen in a 5:1 solution of corn oil and ethanol was prepared as previously described (Berg et al., 2019). In order to dissolve the tamoxifen in the corn oil and ethanol solution, it was heated to 37°C with intermittent vortexing. Stock concentrations were stored at -80°C. Prior to use, tamoxifen was warmed to 37°C and then injected into the intraperitoneal space of P56 to P84 *Nes-CreER:mTmG* animals with or without *Cyfip1* floxed at a final concentration of 248 mg/kg body weight. Animals underwent intracardiac perfusion with 4% PFA 2 to 8 days post injection.

Image Acquisition, Processing, and Quantification

Brain sections were imaged on either a Zeiss LSM 800, a Zeiss LSM 710, or a Zeiss 800 Airyscan confocal microscope (ZEISS International) using Zen Software (ZEISS International). Low magnification images were acquired with 10X or 20X air objectives. High magnification images were acquired with 40X or 63X oil immersion objectives. Z-stacks were obtained using the optimal inter-slice distance for the objective. For quantitative and qualitative experiments in which a control and an experimental condition were being compared, equal settings of laser intensity, pinhole aperture, and inter slice distance for Z-stacks were maintained as constant between conditions within the same experiment whenever possible. For larger fields of view, multiple tiled sections were obtained and stitched together prior to exporting for analysis. 3D reconstructions were generating using Imaris Software 7.6 (Bitplane). Quantification of fluorescence intensity was measured in Adobe Photoshop (Adobe) or Image J software (NIH). Quantification of the number of cells expressing different cell markers was determined using Imaris 7.6, Zen, or Image J software.

Image preparation was conducted in Adobe Photoshop (Adobe). Any modifications to brightness or contrast of images was applied equally to control and experimental images.

Quantification and Statistical Analyses

All data are presented as the mean ± standard error of the means (s.e.m.) for single comparisons using t-tests. For experiments with multiple comparisons and for paired analysis, the mean difference ± standard error of the differences was reported. Unless otherwise noted in the results, in cases where coronal sections were analyzed quantitatively, the average of three sections spaced 240 µm apart was determined for each animal in the experimental population and “n” refers to number of animals. Quantification was performed by a person who was blinded to the animal genotype at the time of imaging and quantification for all figures. Statistical analysis was performed using GraphPad Prism 7 (GraphPad Software Inc.). For experiments with only 2 conditions, a two-tailed Student’s t- test was used for statistical analysis. Unless otherwise noted in the results and figure legends, data were unpaired. For comparisons between multiple groups, a one-way ANOVA followed by the appropriate multiple comparisons tests were used (Sidak’s for comparison between groups, Tukey’s for comparison with a control or single value). P values reported were * for $p < 0.05$, ** for $p < 0.01$, *** for $p < 0.001$, **** for $p < 0.0001$, and NS for $p > 0.05$. Sample sizes were not predetermined using statistical methods. The percent margin of error based on published standard deviations from similar studies for a 95% confidence interval is 5.5% for n = 3 and 3.3% for n = 8 animals per condition.

RESULTS

Cyfip1 expression persists in the neurogenic niche of the adult subventricular zone (SVZ)

To determine whether Cyfip1 is persistently expressed in the neurogenic niche of the adult SVZ, we examined whole-mount preparations as well as coronal sections from C57/Bl6 mice between postnatal day 56 and 70 (Figure 1A). The SVZ niche at this age is characterized by a unique

organization. Type B1 cells express the intermediate filament protein glial fibrillary acidic protein (GFAP) (Garcia et al., 2004). B1 cells send $GFAP^+$ apical projections to the ventricular surface forming the hub of the neurogenic niche architecture (Figure 1B) (Mirzadeh et al., 2008). When viewed *en face* from the ventricular surface in whole-mount preparations (Figure 1C-D, surface; and 1E, 5 µm below the surface), the apical processes of the $GFAP^+$ B1 cells (Figure 1B, "b" and Figure 1C, arrowhead) are surrounded by epithelial-like ependymal cells containing γ-$Tubulin^+$ cilia (Figure 1B, "e1" and "e2"; Figure 1C, arrow) forming a "pinwheel" structure. Cell-cell junctions are demarcated by β-Catenin or N-Cadherin localized to adherens junctions (Figure 1C and 1E). Cell bodies of B1 cells lie beneath the ventricular surface in the SVZ (Figure 1B and 1E).

Immunostaining for Cyfip1 demonstrates that it is expressed in the SVZ of the adult mouse (Figure 1D-F). The expression is at the highest levels in B1 cells and is localized to the apical processes of B1 cells at the ventricular surface (Figure 1D, arrowheads) as well as cell bodies of B1 cells below the surface (Figure 1E). It is localized to GFAP expressing cells in discrete clusters at the surface (Figure 1D, arrowheads). Below the ventricular surface, Cyfip1 staining is present in the cell bodies of $GFAP^+$ cells and overlaps with N-Cadherin immunostaining at cell membranes (Figure 1E) and at lower levels in the $S100\beta^+GFAP^+$ cells (Figure 1F), which represent mature astrocytes (A). In contrast, there is no detectable Cyfip1 expression in the majority of $S100\beta^+GFAP^-$ ependymal cells (E) at the ventricular surface (Figure 1F, arrowheads). This specific expression in $GFAP^+$ cells and exclusion from ependymal cells was confirmed with quantification (B1 vs. E mean difference = 0.725, 95% confidence interval of difference (CI) [0.557, 0.893], $p < 0.0001$; A vs. E mean difference = 0.633, 95% CI [0.465, 0.801], $p < 0.0001$; B1 vs. A mean difference = 0.0925, 95% CI [-0.075, 0.2604], $p = 0.339$; one-way ANOVA followed by Tukey's multiple comparisons test; 616 cells from n = 5 mice; Figure 1G). This result indicates that Cyfip1 is persistently expressed and is specifically restricted to the $GFAP^+$ B1 cells and astrocytes of the adult SVZ.

Loss of Cyfip1 expression alters the cellular composition of the ventricular surface in adult mice

Persistent expression of the Cyfip1 protein in the adult SVZ and the preferential localization of Cyfip1 to B1 cells at the center of the pinwheel niche suggests its potential role in regulating B1 cells in the adult niche. Germ line deletion of C*yfip1* is embryonic lethal (Pathania et al., 2014). Therefore, we generated a conditional knockout animal using *Cyfip1*$^{f/f}$ animals and a *Cre-lox* system in which Cre expression is driven by the *Nestin* promoter that becomes active in NSCs and neural progenitor cells during embryonic brain development (Giusti et al., 2014).

Examination of the lateral ventricular surface of the *Nestin-Cre*:*Cyfip1*$^{f/f}$ conditional knockout adult animals (cKO) compared to littermate controls (Con) carrying the *Cyfip1*$^{f/f}$ alleles, but not expressing Cre, reveals significant changes in the cellular organization at the ventricular surface (Figure 2A). In whole-mount sections, there appears to be an increase in the number of GFAP^{+} cell bodies at the ventricular surface of the cKO animals compared to the controls. Additionally, compared to the control SVZ, where there is prominent GFAP immunoreactivity in the apical processes of B1 cells, the ventricular-projecting processes are not as clearly demarcated in the cKO SVZ. There is also a change in β-Catenin expression at the ventricular surface with less uniform immunostaining at cell-cell junctions (Figure 2A).

We next examined coronal sections of control and cKO adult animals in order to more clearly define changes in the cellular composition and organization observed in the whole-mount preparations. Immunostaining with antibodies directed towards GFAP, S100β, and β-Catenin demonstrates an increase in the number of GFAP^{+} cell bodies of type B1 NSCs in the SVZ and at the ventricular surface (Figure 2B). In the control animals, the majority of cells along the ventricular surface are S100β^{+}GFAP^{-} ependymal cells, while GFAP^{+} B1 cells and astrocytes typically lie below the surface in the SVZ (Figure 2B). In the cKO animals, there is a marked increase in GFAP^{+} cells at the surface (Figure 2B, bottom, left of red line). Additionally, when the numbers of each cell type are quantified in proportion to the total number of cells in the SVZ and at the VZ, the relative

proportion of GFAP$^+$S100β$^-$ type B1 cells is increased in the cKO animals compared to the controls. There is no difference in the number of GFAP$^+$S100β$^+$ astrocytes and GFAP$^-$S100β$^+$ ependymal cells (B1 Control vs. cKO mean difference = -0.17, 95% CI [-0.265, -0.7526], $p < 0.005$; E Control vs. cKO mean difference = 0.075, 95% CI [-0.020, 0.017], $p = 0.159$; A Control vs. cKO mean difference = 0.042, 95% CI [-0.034, 0.052], $p = 0.609$; n = 5 animals per condition; one-way ANOVA followed by Sidak's multiple comparisons test; Figure 2C). These data demonstrate a change in the cellular composition of the SVZ and ventricular surface. The increase in the number of B1 cells at the surface suggests either a translocation of cells to the ventricular surface from beneath, an expansion of the population of cells at the surface, or both.

Loss of Cyfip1 increases proliferating cells at the ventricular surface of adult animals

We hypothesized that the increase in GFAP$^+$ B1 cells at the ventricular surface is the result of the GFAP$^+$ NSCs translocating to the ventricular surface and dividing there. To test this hypothesis, we performed 5-ethynyl-2'-deoxyuridine (EDU) incorporation experiments to label actively cycling cells in the S phase. We injected 56 to 70 day old control animals as well as littermate cKO animals with a single intraperitoneal dose of 200 mg/kg bodyweight of EDU. After 24 hours, whole-mount and coronal sections were used for immunostaining, EDU labeling and quantification. In the whole-mount preparations, there is a significant increase in the number of EDU$^+$ nuclei at the ventricular surface in the cKO animals compared to controls (Con = 316 ± 67 cells/mm^2, n = 3 animals vs. cKO = 782 ± 49 cells/mm^2, n = 3 animals; $p < 0.05$; unpaired t-test; Figure 3A and 3B), indicating an increase in proliferation of cells at or near the ventricular surface.

As the whole-mount preparations only allow visualization of the lateral wall of the lateral ventricle, we also examined coronal preparations of 56 to 70 day-old animals at 24 hours after EDU injection. The number of EDU$^+$ cells at the ventricular surface and in the SVZ was quantified by counting the total number of EDU$^+$ cells lining the lateral wall, the medial wall, and the dorsal wall of the ventricle in every 6th 40 µm coronal section from the first section containing the anterior SVZ to

the posterior SVZ at the level of the dentate gyrus for each animal (Figure 3C-D). As in the whole-mount preparations, there is an increase in EDU^+ cells in the cKO animals compared to the controls (Total cKO vs. Con mean of differences = 360 ± 62.1 cells per hemisphere; n = 5 animals, $p < 0.005$; paired two-tailed t-test; Figure 3D). This increase is reflective of significant increases in proliferating cells independently in the lateral wall (Lateral cKO vs. Con mean of difference = 252 ± 69.9 cells per hemisphere; n = 5 animals, $p < 0.05$; two-tailed paired t-test), the dorsal wall (Dorsal cKO vs. Con mean of difference = 39.8 ± 12.72 cells per hemisphere; n = 5 animals, $p < 0.05$; paired two-tailed t-test), and the medial wall (Medial cKO vs. Con mean of difference = 81.8 ± 26.42 cells per hemisphere; n = 5 animals, $p < 0.05$; paired two-tailed t-test) (Figure 3D). The number of EDU^+ cells in the rostral migratory stream (RMS) just anterior to the ventricles was also independently quantified and shows an increase in the cKO animals (RMS cKO vs. Con mean of difference = 121.3 ± 23.35 cells per hemisphere; n = 5 animals, $p < 0.05$; paired two-tailed t-test; Figure 3D). This increase in the number of EDU^+ cells entering the proximal RMS supports an increase in the generation of new cells rather than a failure to migrate from the ventricular surface.

Acute loss of *Cyfip1* in the adult SVZ disrupts niche architecture and alters NSC proliferation

Studies up to this point have examined the effect of loss of *Cyfip1* during embryonic development and therefore cannot distinguish between the downstream effects of altering the embryonic neurogenic niche or a persistent need for Cyfip1 in the adult niche. To determine whether Cyfip1 plays a persistent functional role in the adult neurogenic niche, we developed an inducible conditional knockout animal (icKO) to delete the *Cyfip1* gene specifically in the NSCs in the SVZ of adult animals after the niche is already established. We used a tamoxifen inducible C*re-lox* system in which expression of a Cre recombinase protein with an estrogen receptor motif (Cre-ER) is driven by the *Nestin* promotor (Balordi and Fishell, 2007). To verify Cre expression and to label cells in which recombination occurred, *Nestin-CreER* animals were crossed with the *mTmG* reporter mouse (Muzumdar et al., 2007).

Adult control animals containing the *Nestin-Cre*ER*:Cyfip1*$^{+/+}$*:mTmG* transgenes that were wild type for *Cyfip1* (Control), as well as animals with a *Nestin-Cre*ER*:Cyfip1*$^{f/f}$*:mTmG* genotype (icKO) were injected with tamoxifen between P56 and P84. Animals were then sacrificed at 2, 4 and 8 days post injection (DPI) for analysis. Animals sacrificed at 8 DPI demonstrated decreased levels of Cyfip1 protein in the GFAP$^+$ cells beneath the cell surface (Figure 4A). Quantification of the relative immunofluorescence levels for Cyfip1 showed approximately 45% of controls in icKO animals (mean Cyfip1 immunofluorescence intensity 49.5 ± 5.5 intensity units, n = 5 Control cells vs. 22.2 ± 4.1 intensity units, n = 13 icKO cells; p = 0.002; unpaired t-test). Whole-mount immunostaining with antibodies targeted against GFP, marking recombined mTmG$^+$ cells, indicates that as early as 2 DPI Cre-mediated recombination occurs at similar frequencies in both the control and icKO animals. There is an increase in the intensity of GFP immunofluorescence by 4 and 8 DPI in both conditions (Figure 4B).

To determine whether Cyfip1 is required for regulation of the SVZ niche, we examined GFAP expression as well as N-Cadherin expression at the ventricular surface after tamoxifen induction. At 8 DPI, there is a marked increase in the number of GFAP$^+$ cells at the ventricular surface (Figure 5A and 5B). This increase in GFAP immunoreactivity occurs in the form of an increased number of apical process clusters as well as an increased number of cell bodies at the cell surface and is reflective of a significant increase in the number of normal and abnormal pinwheel formations (icKO vs. Con mean of differences = 7.95 ± 1.37 GFAP$^+$ cells/100 mm^2, $p < 0.05$, paired two-tailed t-test; Figure 5B). When the expression of N-Cadherin and GFAP in the pinwheel formations is examined at a high magnification in the control SVZ, there is a distinct demarcation between the GFAP$^+$ apical projections and the ependymal cells at the surface with very little overlap between GFAP and N-Cadherin immunostaining, and intense N-Cadherin immunostaining surrounding the central apical projections (Figure 5C, Control, arrowheads). In contrast, there is a marked overlap in N-cadherin and GFAP expression in the iCKO animals at 8 DPI. In the absence of Cyfip1, N-Cadherin is no longer excluded from the center of the apical

projection and there is no longer a clear demarcation between B1 cells and non-GFAP expressing cells at the surface (Figure 5C, 8 DPI, arrowheads). Additionally, cell-cell junctions along the surface are thicker and less clearly defined compared to the controls. At 2 and 4 DPI, some of the $GFAP^+$ projections of the icKO animals are similar to the control animals. In others, the phenotype is similar to the $GFAP^+$ processes of the 8 DPI icKO animals (Figure 5C). These results indicate that the structural changes begin prior to the 8 DPI time point.

We further examined the effect of acute *Cyfip1* deletion on the cellular distribution of the SVZ niche in coronal sections from tamoxifen injected mice at 8 DPI. Cells were immunostained for GFP, GFAP and S100β in order to determine the relative number of $GFAP^+S100\beta^-$ B1 cells, $GFAP^-S100\beta^+$ ependymal cells and $GFAP^+S100\beta^+$ astrocytes compared to the total GFP^+ recombined cells at the ventricular surface and in the SVZ (Figure 6A). Similar to the cKO animals in which *Cyfip1* is deleted from the embryonic NSCs, there is a significant increase in the number of $GFAP^+S100\beta^-$ B1 cells relative to total cells in the icKO animals compared to controls (B1 Con vs. icKO mean difference = -0.121, 95% CI [-0.235, -0.008], n = 7 animals per condition, $p < 0.05$; one-way ANOVA followed by Sidak's multiple comparisons test; Figure 6B). There was not a significant change in either the number of ependymal cells or astrocytes (E Con vs. icKO mean difference = 0.03552, 95% CI [-0.078, 0.148], p = 0.821; A Con vs. icKO mean difference = -0.017, 95% CI [-0.130, 0.096], p = 0.976; n = 7 animals per condition; one-way ANOVA followed by Sidak's multiple comparisons test; Figure 6B). These results suggest that Cyfip1 specifically regulates the number of $GFAP^+S100\beta^-$ B1 cells at the ventricular surface and in the SVZ.

To determine whether there is an increase in the proliferation of B1 cells within the niche, we injected P56-P84 control and icKO animals with tamoxifen, followed by injection with EDU at 2 hours prior to perfusion at 8 DPI. Coronal sections were subsequently immunostained with antibodies against Sox2, a transcription factor expressed in B1 cells, and GFP (Figure 7A). Consistent with the results of $GFAP^+$ B1 cell quantification, there was a proportional increase in the number of $Sox2^+GFP^+$ cells relative to all GFP^+ cells in the icKO animals compared to the controls

(Con vs. icKO mean difference = -0.192, 95% CI [-0.289, -0.094], n = 4 animals per condition, $p < 0.001$; one-way ANOVA followed by Sidak's multiple comparisons test; Figure 7B). Additionally, there was an increase in the number of $Sox2^+GFP^+EDU^+$ cells in the icKO compared to control animals (Con vs. icKO mean difference = -0.147, 95% CI [-0.227, -0.003], n = 3 animals per condition, $p < 0.05$; one-way ANOVA followed by Sidak's multiple comparisons test; Figure 7B). These results indicate that there are more $Sox2^+$ B1 cells and they exhibit a higher rate of proliferation upon *Cyfip1* deletion.

Previous studies have shown that B1 cell division in the SVZ leads to either a symmetric expansion of B1 cells or to neurogenic cell divisions (Obernier et al., 2018). In order to assess whether the increased divisions that occur in the absence of *Cyfip1* are self-renewing or neurogenic or a combination of both, 8 DPI coronal sections from control and icKO animals were immunostained for Mash1, a transcription factor expressed in transient amplifying cells (TACs) (Figure 7C), and Doublecortin (Dcx), a microtubule-associated protein expressed in neuroblasts (Figure 7D). In contrast to the $Sox2^+$ cells, there was no significant change in the proportion of $Mash1^+$ TACs among GFP^+ cells in the icKO compared to the controls (Con = 0.103 ± 0.025, n = 6 animals; icKO = 0.117 ± 0.009, n = 8 animals; p = 0.5, two-tailed t-test; Figure 7E, left). Similarly, there was no difference between the proportion of Dcx^+GFP^+ neuroblasts among GFP^+ cells in control and icKO animals (Con = 0.297 ± 0.011, n = 7 animals; icKO = 0.312 ± 0.019, n = 8 animals; p = 0.5, two-tailed t-test; Figure 7E, right). Together, these data indicate that acute loss of *Cyfip1* does not lead to an increase in cells with a neurogenic fate and support the hypothesis that the increased B1 cell divisions upon *Cyfip1* deletion are symmetric self-renewing.

DISCUSSION

In this study, we demonstrate that Cyfip1 is important for proper establishment and maintenance of the adult SVZ niche architecture and regulation of type B1 cell proliferation and localization. While the importance of Cyfip1 in embryonic development and mature neuronal plasticity is beginning to

be appreciated (Abekhoukh and Bardoni, 2014; Abekhoukh et al., 2017; Yoon et al., 2014; De Rubeis et al., 2013), this study is the first to suggest that Cyfip1 is a critical component in establishing and maintaining the adult SVZ NSC niche and regulating adult NSC fate. Our study further suggests that type B1 adult NSCs maintain the capacity for symmetric self-renewal to amplify their pool in the adult brain.

In contrast to the embryonic period, where there is prominent Cyfip1 expression in the apical membranes of RGCs covering the entire ventricular surface (Yoon et al., 2014), our study demonstrates that the overall expression of Cyfip1 at the ventricular surface decreases in the adult SVZ as RGCs differentiate into ependymal cells. Remarkably, this indicates an expression specificity for NSCs as Cyfip1 continues to be expressed in the $GFAP^+$ type B1 NSCs and is not prominent in the $S100\beta^+GFAP^-$ mature ependymal cells. Similar to what is seen in the RGCs of embryonic development, there is specific localization of this protein to the apical processes at the ventricular surface in the adult SVZ and overlap with N-Cadherin expression at cell-cell junctions. As is the case in embryonic development, Cyfip1 is involved in the regulation of adherens junctions in the adult SVZ and is required for NSC niche maintenance.

Mirzedah et al (2008) have previously shown by electron microscopy that adherens junctions in the pinwheel formations of the adult SVZ are asymmetric between ependymal cells and type B1 cells. Junctions between B1 cells are similar to those seen between RGCs in development. Ependymal-ependymal cell junctions are different from both (Mirzadeh et al., 2008). Asymmetric persistence of Cyfip1 expression and the resultant differential regulation of adherens junctions in B1 cells, but not in ependymal cells, is one potential mechanism leading to B1 cell specific adherens junctions. In support of this notion, in the control SVZ, there is a discrete localization of N-Cadherin to the cell-cell junctions in B1 cells. Acute deletion of *Cyfip1* results in a dispersion of N-Cadherin from a discrete apical membrane ring surrounding $GFAP^+$ processes, suggesting that Cyfip1 stabilizes N-Cadherin at the apical cell-cell junction.

In the embryonic NSC niche, disrupted adherens junction stability leads to shorter cell cycles and a reduction of cells that exit the cell cycle (Gil-Sanz et al., 2014). Here, we observed an increase in cell division as well as an increase in the number of B1 cells in the adult SVZ as a consequence of loss of *Cyfip1* during the embryonic stages. Previous work has demonstrated that B1 cell divisions in the adult SVZ are either symmetrically self-depleting or symmetrically self-renewing and the balance between the two favors depletion over time, leading to a progressive decrease in B1 cells with aging (Obernier et al., 2018). An increase in cell divisions can either lead to depletion or expansion of the overall NSC pool depending on which type of division is enhanced. In another model examining niche regulation of B1 cell division in the adult SVZ, loss of apical end feet anchoring in the niche by blocking vascular molecular adhesion molecule-1 (VCAM-1) leads to disrupted pinwheel architecture and increased self-depleting neurogenic divisions with a resultant depletion of B1 cells (Kokovay et al., 2012). In contrast, in this study, we found increased self-renewing proliferation and a specific expansion of B1 cells upon *Cyfip1* deletion.

In the conditional knockout model (cKO), it is possible that loss of *Cyfip1* during embryonic development alters the structure of the niche and it is the dysregulated niche, but not a persistent need for Cyfip1 in the adult niche, that contributes to the observed effects. However, the marked loss of localization of N-Cadherin to cell-cell junctions, accompanied by the expansion of type B1 cells, and an increase in their proliferation when *Cyfip1* is acutely depleted in our inducible conditional (icKO) model indicates that persistent Cyfip1 expression in B1 cells is indeed required to maintain the niche. Furthermore, the upregulation of self-renewing proliferation after acute deletion of *Cyfip1* without an increase in transient amplifying cells or neuroblasts indicates that there is not an immediate increase in neurogenesis as a result of the acute loss of *Cyfip1*. This result suggests that it is possible to attenuate or reverse the progressive depletion of B1 cells in the adult SVZ of control animals and that normal levels of Cyfip1 protein expression are required to regulate fate choices and maintain the balance between renewing and depleting neurogenic divisions of B1 cells.

The exact mechanisms by which Cyfip1 regulates these processes are unclear. It is possible that the symmetric vs. asymmetric adherens junctions provide information to B1 cells about the surrounding cells and the loss of adhesion acts as a signal to B1 cells to generate new cells through division. Alternatively, Cyfip1 may regulate cell fate choice through a signaling mechanism independent of its role in adherens junction maintenance and further studies are needed to elucidate which of these hypotheses is correct. In contrast to the acute ickO model in which there is no increase in neuroblasts, when *Cyfip1* is lost during the embryonic stage in the cKO model, there is an increase in cycling cells in the RMS. We hypothesize that *Cyfip1* knockout in neural progenitor cells during embryonic development would lead to subsequent early expansion of the B1 cell population. Because *Cyfip1* knockout does not completely stop neurogenic divisions, there are more B1 cells later in the adult SVZ that are available to generate new neurons which would potentially lead to an increase in the number of cells in the RMS. Understanding the regulation of this later fate determination will be important to understanding both normal and pathologic development.

The potential of B1 cells in the adult to reactivate their capacity for symmetric self-renewing divisions after embryonic development could have implications for regeneration as well as oncologic transformation. With regards to the latter possibility, it should be noted that CYFIP1 has been proposed as a tumor invasion suppressor in humans (Silva, J. M. et al., 2009). Additionally, the phenotype observed in our cKO model demonstrating increased symmetric renewing divisions in the adult after embryonic deletion is pertinent to recent findings demonstrating that humans who are haploinsufficient for *CYFIP1* due to deletion of the 15q11.2 locus, where the gene is located, have microstructural alterations in the white matter as detected by MRI (Silva, A. I. et al., 2019). Additionally, mice that are haploinsufficient for *Cyfip1* have decreased myelination in the corpus callosum and decreased numbers of oligodendrocytes and abnormal behavior (Silva, A. I. et al., 2019; Dominguez-Iturza et al., 2019). Although there are many hypotheses as to why loss of *Cyfip1* in mice could alter myelination based on its known role in actin nucleation, which is necessary for

515 migration and adhesion, the data presented here suggest the possibility that the increased
516 symmetric B1 cell renewing divisions could occur at the expense of the generation of
517 oligodendrocytes, resulting in impaired myelination either in the pre- or postnatal period or both.
518 *CYFIP1* is located within the 15q11.2 locus in humans and deletions or duplications in this
519 region are found in patients with epilepsy, intellectual disability, autism and schizophrenia (van der
520 Zwaag et al., 2010; von der Lippe et al., 2011; Doornbos et al., 2009; Borlot et al., 2017; Mullen et
521 al., 2013; Mefford et al., 2010; de Kovel et al., 2010; Rudd et al., 2014). Copy number variation in
522 the 15q11.2 locus also results in changes in white matter microstructure (Silva, A. I. et al., 2019).
523 The role of Cyfip1 as a member of the WAVE regulatory complex (WRC) in regulating actin
524 nucleation makes it an ideal candidate to regulate synaptic plasticity as well as early neural
525 development (Abekhoukh et al., 2017; Yoon et al., 2014; De Rubeis et al., 2013). Results presented
526 here suggest that it continues to be important in postnatal NSC regulation with potentially important
527 downstream effects on postnatal neuron and oligodendrocyte genesis. Building on the previous
528 finding of the necessity of Cyfip1 for the establishment of apical basal polarity in embryonic
529 neurogenesis (Yoon et al., 2014), this study reveals a persistent requirement for its expression in
530 the adult neurogenic niche. Together, these results indicate that Cyfip1 is crucial to NSC behavior
531 and the neurogenic niche throughout life. Importantly, we show that Cyfip1 suppresses self-
532 renewing B1 cell divisions and that NSCs can be reactivated to favor self-renewal even in the adult
533 SVZ.
534

REFERENCES

Abekhoukh S, Bardoni B (2014) CYFIP family proteins between autism and intellectual disability: Links with fragile X syndrome. Front Cell Neurosci (Switzerland) 8:81.

Abekhoukh S et al (2017) New insights into the regulatory function of CYFIP1 in the context of WAVE- and FMRP-containing complexes. Dis Model Mech (England) 10:463-474.

Altman J (1969) Autoradiographic and histological studies of postnatal neurogenesis. IV. Cell proliferation and migration in the anterior forebrain, with special reference to persisting neurogenesis in the olfactory bulb. J Comp Neurol (United States) 137:433-457.

Alvarez-Buylla A, Lim DA (2004) For the long run: Maintaining germinal niches in the adult brain. Neuron (United States) 41:683-686.

Balordi F, Fishell G (2007) Mosaic removal of hedgehog signaling in the adult SVZ reveals that the residual wild-type stem cells have a limited capacity for self-renewal. J Neurosci (United States) 27:14248-14259.

Berg DA, Su Y, Jimenez-Cyrus D, Patel A, Huang N, Morizet D, Lee S, Shah R, Ringeling FR, Jain R, Epstein JA, Wu QF, Canzar S, Ming GL, Song H, Bond AM (2019) A common embryonic origin of stem cells drives developmental and adult neurogenesis. Cell (United States) 177:654-668.e15.

Bizzotto S, Francis F (2015) Morphological and functional aspects of progenitors perturbed in cortical malformations. Front Cell Neurosci (Switzerland) 9:30.

Bond AM, Ming GL, Song H (2015) Adult mammalian neural stem cells and neurogenesis: Five decades later. Cell Stem Cell (United States) 17:385-395.

Borlot F, Regan BM, Bassett AS, Stavropoulos DJ, Andrade DM (2017) Prevalence of pathogenic copy number variation in adults with pediatric-onset epilepsy and intellectual disability. JAMA Neurol (United States) 74:1301-1311.

de Kovel CG et al (2010) Recurrent microdeletions at 15q11.2 and 16p13.11 predispose to idiopathic generalized epilepsies. Brain (England) 133:23-32.

De Rubeis S, Pasciuto E, Li KW, Fernandez E, Di Marino D, Buzzi A, Ostroff LE, Klann E, Zwartkruis FJ, Komiyama NH, Grant SG, Poujol C, Choquet D, Achsel T, Posthuma D, Smit AB, Bagni C (2013) CYFIP1 coordinates mRNA translation and cytoskeleton remodeling to ensure proper dendritic spine formation. Neuron (United States) 79:1169-1182.

Doetsch F, Caille I, Lim DA, Garcia-Verdugo JM, Alvarez-Buylla A (1999) Subventricular zone astrocytes are neural stem cells in the adult mammalian brain. Cell (United States) 97:703-716.

Dominguez-Iturza N, Lo AC, Shah D, Armendariz M, Vannelli A, Mercaldo V, Trusel M, Li KW, Gastaldo D, Santos AR, Callaerts-Vegh Z, D'Hooge R, Mameli M, Van der Linden A, Smit AB, Achsel T, Bagni C (2019) The autism- and schizophrenia-associated protein CYFIP1 regulates bilateral brain connectivity and behaviour. Nat Commun (England) 10:3454-019-11203-y.

Doornbos M, Sikkema-Raddatz B, Ruijvenkamp CA, Dijkhuizen T, Bijlsma EK, Gijsbers AC, Hilhorst-Hofstee Y, Hordijk R, Verbruggen KT, Kerstjens-Frederikse WS, van Essen T, Kok K, van

572 Silfhout AT, Breuning M, van Ravenswaaij-Arts CM (2009) Nine patients with a microdeletion
573 15q11.2 between breakpoints 1 and 2 of the prader-willi critical region, possibly associated with
574 behavioural disturbances. Eur J Med Genet (Netherlands) 52:108-115.

575 Ferland RJ, Batiz LF, Neal J, Lian G, Bundock E, Lu J, Hsiao YC, Diamond R, Mei D, Banham AH,
576 Brown PJ, Vanderburg CR, Joseph J, Hecht JL, Folkerth R, Guerrini R, Walsh CA, Rodriguez EM,
577 Sheen VL (2009) Disruption of neural progenitors along the ventricular and subventricular zones in
578 periventricular heterotopia. Hum Mol Genet (England) 18:497-516.

579 Garcia AD, Doan NB, Imura T, Bush TG, Sofroniew MV (2004) GFAP-expressing progenitors are
580 the principal source of constitutive neurogenesis in adult mouse forebrain. Nat Neurosci (United
581 States) 7:1233-1241.

582 Gil-Sanz C, Landeira B, Ramos C, Costa MR, Muller U (2014) Proliferative defects and formation of
583 a double cortex in mice lacking Mltt4 and Cdh2 in the dorsal telencephalon. J Neurosci (United
584 States) 34:10475-10487.

585 Giusti SA, Vercelli CA, Vogl AM, Kolarz AW, Pino NS, Deussing JM, Refojo D (2014) Behavioral
586 phenotyping of nestin-cre mice: Implications for genetic mouse models of psychiatric disorders. J
587 Psychiatr Res (England) 55:87-95.

588 Gotz M, Huttner WB (2005) The cell biology of neurogenesis. Nat Rev Mol Cell Biol (England)
589 6:777-788.

590 Guerra MM, Henzi R, Ortloff A, Lichtin N, Vio K, Jimenez AJ, Dominguez-Pinos MD, Gonzalez C,
591 Jara MC, Hinostroza F, Rodriguez S, Jara M, Ortega E, Guerra F, Sival DA, den Dunnen WF,
592 Perez-Figares JM, McAllister JP, Johanson CE, Rodriguez EM (2015) Cell junction pathology of
593 neural stem cells is associated with ventricular zone disruption, hydrocephalus, and abnormal
594 neurogenesis. J Neuropathol Exp Neurol (England) 74:653-671.

595 Jimenez AJ, Garcia-Verdugo JM, Gonzalez CA, Batiz LF, Rodriguez-Perez LM, Paez P, Soriano-
596 Navarro M, Roales-Bujan R, Rivera P, Rodriguez S, Rodriguez EM, Perez-Figares JM (2009)
597 Disruption of the neurogenic niche in the subventricular zone of postnatal hydrocephalic hyh mice. J
598 Neuropathol Exp Neurol (England) 68:1006-1020.

599 Kokovay E, Wang Y, Kusek G, Wurster R, Lederman P, Lowry N, Shen Q, Temple S (2012)
600 VCAM1 is essential to maintain the structure of the SVZ niche and acts as an environmental sensor
601 to regulate SVZ lineage progression. Cell Stem Cell (United States) 11:220-230.

602 Kosodo Y, Roper K, Haubensak W, Marzesco AM, Corbeil D, Huttner WB (2004) Asymmetric
603 distribution of the apical plasma membrane during neurogenic divisions of mammalian
604 neuroepithelial cells. Embo J (England) 23:2314-2324.

605 Lian G, Sheen VL (2015) Cytoskeletal proteins in cortical development and disease: Actin
606 associated proteins in periventricular heterotopia. Front Cell Neurosci (Switzerland) 9:99.

607 Liu P, Jenkins NA, Copeland NG (2003) A highly efficient recombineering-based method for
608 generating conditional knockout mutations. Genome Res (United States) 13:476-484.

609 Lois C, Alvarez-Buylla A (1994) Long-distance neuronal migration in the adult mammalian brain.
610 Science (United States) 264:1145-1148.

611 Lois C, Alvarez-Buylla A (1993) Proliferating subventricular zone cells in the adult mammalian
612 forebrain can differentiate into neurons and glia. Proc Natl Acad Sci U S A (United States) 90:2074-
613 2077.

614 Mefford HC, Muhle H, Ostertag P, von Spiczak S, Buysse K, Baker C, Franke A, Malafosse A,
615 Genton P, Thomas P, Gurnett CA, Schreiber S, Bassuk AG, Guipponi M, Stephani U, Helbig I,
616 Eichler EE (2010) Genome-wide copy number variation in epilepsy: Novel susceptibility loci in
617 idiopathic generalized and focal epilepsies. PLoS Genet (United States) 6:e1000962.

618 Menn B, Garcia-Verdugo JM, Yaschine C, Gonzalez-Perez O, Rowitch D, Alvarez-Buylla A (2006)
619 Origin of oligodendrocytes in the subventricular zone of the adult brain. J Neurosci (United States)
620 26:7907-7918.

621 Mercier F, Kitasako JT, Hatton GI (2002) Anatomy of the brain neurogenic zones revisited:
622 Fractones and the fibroblast/macrophage network. J Comp Neurol (United States) 451:170-188.

623 Mirzadeh Z, Doetsch F, Sawamoto K, Wichterle H, Alvarez-Buylla A (2010) The subventricular zone
624 en-face: Wholemount staining and ependymal flow. J Vis Exp (United States) (39). pii: 1938.
625 doi:10.3791/1938.

626 Mirzadeh Z, Merkle FT, Soriano-Navarro M, Garcia-Verdugo JM, Alvarez-Buylla A (2008) Neural
627 stem cells confer unique pinwheel architecture to the ventricular surface in neurogenic regions of
628 the adult brain. Cell Stem Cell (United States) 3:265-278.

629 Mullen SA, Carvill GL, Bellows S, Bayly MA, Trucks H, Lal D, Sander T, Berkovic SF, Dibbens LM,
630 Scheffer IE, Mefford HC (2013) Copy number variants are frequent in genetic generalized epilepsy
631 with intellectual disability. Neurology (United States) 81:1507-1514.

632 Muzumdar MD, Tasic B, Miyamichi K, Li L, Luo L (2007) A global double-fluorescent cre reporter
633 mouse. Genesis (United States) 45:593-605.

634 Obernier K, Cebrian-Silla A, Thomson M, Parraguez JI, Anderson R, Guinto C, Rodas Rodriguez J,
635 Garcia-Verdugo JM, Alvarez-Buylla A (2018) Adult neurogenesis is sustained by symmetric self-
636 renewal and differentiation. Cell Stem Cell (United States) 22:221-234.e8.

637 O'Leary CJ, Nourse CC, Lee NK, White A, Langford M, Sempert K, Cole SJ, Cooper HM (2017)
638 Neogenin recruitment of the WAVE regulatory complex to ependymal and radial progenitor
639 adherens junctions prevents hydrocephalus. Cell Rep (United States) 20:370-383.

640 Parras CM, Galli R, Britz O, Soares S, Galichet C, Battiste J, Johnson JE, Nakafuku M, Vescovi A,
641 Guillemot F (2004) Mash1 specifies neurons and oligodendrocytes in the postnatal brain. Embo J
642 (England) 23:4495-4505.

643 Pathania M, Davenport EC, Muir J, Sheehan DF, Lopez-Domenech G, Kittler JT (2014) The autism
644 and schizophrenia associated gene CYFIP1 is critical for the maintenance of dendritic complexity
645 and the stabilization of mature spines. Transl Psychiatry (United States) 4:e374.

646 Priya R, Yap AS (2015) Active tension: The role of cadherin adhesion and signaling in generating
647 junctional contractility. Curr Top Dev Biol (United States) 112:65-102.

Relucio J, Menezes MJ, Miyagoe-Suzuki Y, Takeda S, Colognato H (2012) Laminin regulates postnatal oligodendrocyte production by promoting oligodendrocyte progenitor survival in the subventricular zone. Glia (United States) 60:1451-1467.

Rousselot P, Lois C, Alvarez-Buylla A (1995) Embryonic (PSA) N-CAM reveals chains of migrating neuroblasts between the lateral ventricle and the olfactory bulb of adult mice. J Comp Neurol (United States) 351:51-61.

Rudd DS, Axelsen M, Epping EA, Andreasen NC, Wassink TH (2014) A genome-wide CNV analysis of schizophrenia reveals a potential role for a multiple-hit model. Am J Med Genet B Neuropsychiatr Genet (United States) 165B:619-626.

Shook BA, Manz DH, Peters JJ, Kang S, Conover JC (2012) Spatiotemporal changes to the subventricular zone stem cell pool through aging. J Neurosci (United States) 32:6947-6956.

Silva AI, Ulfarsson MO, Stefansson H, Gustafsson O, Walters GB, Linden DEJ, Wilkinson LS, Drakesmith M, Owen MJ, Hall J, Stefansson K (2019) Reciprocal white matter changes associated with copy number variation at 15q11.2 BP1-BP2: A diffusion tensor imaging study. Biol Psychiatry (United States) 85:563-572.

Silva AI, Haddon JE, Ahmed Syed Y, Trent S, Lin TE, Patel Y, Carter J, Haan N, Honey RC, Humby T, Assaf Y, Owen MJ, Linden DEJ, Hall J, Wilkinson LS (2019) Cyfip1 haploinsufficient rats show white matter changes, myelin thinning, abnormal oligodendrocytes and behavioural inflexibility. Nat Commun (England) 10:3455-019-11119-7.

Silva JM, Ezhkova E, Silva J, Heart S, Castillo M, Campos Y, Castro V, Bonilla F, Cordon-Cardo C, Muthuswamy SK, Powers S, Fuchs E, Hannon GJ (2009) Cyfip1 is a putative invasion suppressor in epithelial cancers. Cell (United States) 137:1047-1061.

Tronche F, Kellendonk C, Kretz O, Gass P, Anlag K, Orban PC, Bock R, Klein R, Schutz G (1999) Disruption of the glucocorticoid receptor gene in the nervous system results in reduced anxiety. Nat Genet (United States) 23:99-103.

van der Zwaag B, Staal WG, Hochstenbach R, Poot M, Spierenburg HA, de Jonge MV, Verbeek NE, van 't Slot R, van Es MA, Staal FJ, Freitag CM, Buizer-Voskamp JE, Nelen MR, van den Berg LH, van Amstel HK, van Engeland H, Burbach JP (2010) A co-segregating microduplication of chromosome 15q11.2 pinpoints two risk genes for autism spectrum disorder. Am J Med Genet B Neuropsychiatr Genet (United States) 153B:960-966.

Verma S, Han SP, Michael M, Gomez GA, Yang Z, Teasdale RD, Ratheesh A, Kovacs EM, Ali RG, Yap AS (2012) A WAVE2-Arp2/3 actin nucleator apparatus supports junctional tension at the epithelial zonula adherens. Mol Biol Cell (United States) 23:4601-4610.

von der Lippe C, Rustad C, Heimdal K, Rodningen OK (2011) 15q11.2 microdeletion - seven new patients with delayed development and/or behavioural problems. Eur J Med Genet (Netherlands) 54:357-360.

Wang PS, Chou FS, Ramachandran S, Xia S, Chen HY, Guo F, Suraneni P, Maher BJ, Li R (2016) Crucial roles of the Arp2/3 complex during mammalian corticogenesis. Development (England) 143:2741-2752.

687 Yoon KJ et al (2014) Modeling a genetic risk for schizophrenia in iPSCs and mice reveals neural
688 stem cell deficits associated with adherens junctions and polarity. Cell Stem Cell (United States)
689 15:79-91.

690

FIGURE LEGENDS

Figure 1. Cyfip1 is expressed in B1 cells of the adult subventricular zone. (A) Diagrammatic illustration of the whole-mount and coronal preparations used for analysis in this study. Gray squares correspond to the region for the 3-dimensional (3D) image in (B). (B) 3D diagram of the cellular composition of the adult subventricular zone (SVZ). e1: E1 ependymal cells. e2: E2 ependymal cells. b: type B1 cells. c: type C transient amplifying cells. a: migratory neuroblasts. Model based on that of Mirzadeh *et al.* 2008. (C) Sample confocal images of the whole-mount preparation of the dorsolateral surface of the lateral ventricle of a control adult animal with immunofluorescent staining for β-Catenin and ɣ-Tubulin (green), GFAP (red), and DAPI (blue) in the merged image. Arrowhead indicates $GFAP^+$ projection at the center of a pinwheel formation. Arrow indicates an ependymal cell forming a blade of the same pinwheel formation. (D) Sample confocal images of immunofluorescent staining of GFAP (blue) and Cyfip1 (red) on the dorsolateral ventricular surface with pictorial representation of the architecture in the last panel. Arrowheads indicate apical $GFAP^+$ projections at the center of the pinwheels. Merged panel is an orthographic projection. (E) Sample confocal images of immunostaining of GFAP (blue), Cyfip1 (red) and N-Cadherin (green) 5 µm below the ventricular surface. Merged panel is an orthographic projection. (F) Sample confocal images of coronal sections immunostained for GFAP (red), Cyfip1 (green), S100β (blue), and DAPI (grey in the merged image). Images are examples from the medial (top) and the lateral (bottom) ventricular walls. Arrowheads indicate $S100\beta^+GFAP^-Cyfip1^-$ ependymal cells surrounded by $Cyfip1^+GFAP^+S100\beta^+$ astrocytes and $Cyfip1^+GFAP^+S100\beta^-$ B1 cells. Scale bars, 20 µm (C-E) and 10 µm (F). All images are representative of similar immunostaining observed in a minimum of 4 animals. (G) Quantification of the number of cells that are $Cyfip1^+$ in each of three cell types in the adult SVZ niche. B1: $GFAP^+S100\beta^-$ type B1 cells, A: $GFAP^+S100\beta^+$ astrocytes, E: $GFAP^-S100\beta^+$ ependymal cells. Ratios represent the total number of each cell type divided by the number of $Cyfip1^+$cells of that type. Quantification is based on 616 cells from coronal sections as in (F) in n = 5 animals. Each dot represents value of the mean from one animal. Bar

values represent the mean of 5 animals ± s.e.m. (****p < 0.0001; one-way ANOVA followed by Tukey's multiple comparisons test).

Figure 2. Loss of *Cyfip1* alters the structure of the ventricular surface in adult *Cyfip1* conditional knockout mice. (A) Sample confocal images of the ventricular surface in control and conditional *Cyfip1* knockout (cKO) adult mice. Whole-mount preparations were immunostained for β-Catenin (green), GFAP (red), and DAPI (blue in merged image). Scale bar, 20 μm. (B) Sample confocal images of coronal sections of the lateral ventricle of the adult SVZ in control versus cKO animals. Sections immunostained with antibodies targeting S100β (red), β-Catenin (green), and GFAP (blue). Red line demarcates the border between the first cell layer at the ventricular surface and the SVZ. Scale bar, 10 μm. (C) Quantification of the cellular composition of the SVZ and ventricular surface. The number of $GFAP^+$ and $S100\beta^+$ cells were quantified in relation to the total number of cells based on nuclear DAPI staining. B1: $GFAP^+S100\beta^-$ type B1 cells, A: $GFAP^+S100\beta^+$ astrocytes, E: $GFAP^-S100\beta^+$ ependymal cells. Each dot represents the mean counts of 3 sections per animal. Bar values represent the mean of the means ± s.e.m. (n = 6 control and 7 cKO animals. ***p < 0.001, NS: p > 0.05; one-way ANOVA followed by Sidak's multiple comparisons test).

Figure 3. Loss of *Cyfip1* during embryonic development results in altered cell proliferation in the adult subventricular zone. (A) Sample images of whole-mount preparations of EDU-injected control and conditional knockout (cKO) adult mice 24 hours post injection. Tiled 3D images were obtained to capture the entire ventricular surface and reconstructed in *Imaris* software. EDU^+ nuclei were marked for quantification (red dots). Scale bar, 500 μm. (B) EDU^+ cells as in (A) were quantified and normalized to the total area of the ventricular surface for each animal as shown as individual dots. Bar values present mean ± s.e.m. (n = 3 animals for each condition; **p < 0.001; paired two-tailed t-test). (C) Sample confocal images of the lateral wall of the lateral ventricles in coronal section from control and cKO animals stained with EDU (red), GFAP (green), and DAPI

(blue). Images are orthogonal reconstructions of a subarea of the ventricular wall similar to the grey box in the inset in (D). Scale bar, 20 μm. (D) Quantification of EDU^+ cells in 40 μm coronal sections. Every 6^{th} section beginning from the posterior frontal lobe just anterior to the ventricle (rostral migratory stream, RMS) and extending to the dentate gyrus of the hippocampus was examined. Each dot represents the value of the total cells quantified for each animal with a minimum of 7 sections along the anterior to posterior axis of the lateral ventricles examined with variation dependent on the size of the ventricle and no difference in number of sections between genotypes. Bars represent the mean of animals ± s.e.m. (n = 5 animals for control and 5 animals for cKO; **p < 0.005; *p < 0.05; paired two-tailed t-test).

Figure 4. Acute deletion of *Cyfip1* in the adult SVZ. (A) Sample confocal images of the ventricular wall of control and induced conditional knockout (icKO) adult animals demonstrating decreased Cyfip1 levels by immunofluorescence. Scale bar, 20 μm. (B) Sample confocal images of N-Cadherin (blue) and GFP (green) immunofluorescence at 2, 4 and 8 days post injection (DPI) in whole-mount preparations in control and icKO mice. Scale bar, 20 μm.

Figure 5. Acute loss of *Cyfip1* disrupts the adult ventricular surface. (A) Sample confocal images of whole-mount preparations from control and induced conditional knockout (icKO) adult animals at 8 days post injection (DPI) that are immunostained for GFP (green), GFAP (red) and N-Cadherin (blue). Arrowheads indicate $GFAP^+$ apical processes at the surface. Scale bar, 20 μm. (B) Quantification of the number of $GFAP^+$ cell contacts at the cell surface of whole-mount preparations. Each dot represents the value from each animal. Bar values present mean ± s.e.m. (n = 4 animals per condition. *p < 0.05; two-tailed paired t-test). (C) Sample confocal high magnification images of whole-mount preparations immunostained for GFAP (red) and N-Cadherin (blue). Arrowheads indicate type B1 cells and ependymal junctions in control versus cKO animals at 2, 4, and 8 DPI. Scale bar, 20 μm.

Figure 6. Acute loss of *Cyfip1* increases the proportion of GFAP$^+$ B1 cells in the adult SVZ. (A) Sample confocal images of coronal sections immunostained for GFAP (red), GFP (green), and S100β (blue) from control and induced conditional knockout (icKO) adult animals. Scale bar, 10 μm. (B) Quantification of GFAP$^+$s100β$^-$ B1 cell (B1), GFAP$^+$s100β$^+$ astrocytes (A), and GFAP$^-$s100β$^+$ ependymal cells (E) expressing GFP compared to the total GFP$^+$ cells at the ventricular surface and in the SVZ of the lateral wall of the lateral ventricles. Each dot represents the mean of 3 sections per animal. Bars represent the mean ± s.e.m (n = 7 animals per condition, *p < 0.05; NS: p > 0.05; one-way ANOVA followed by Sidak's multiple comparisons test).

Figure 7. Acute loss of *Cyfip1* increases proliferating Sox2$^+$ B1 cells, but does not affect the proportion of Mash1$^+$ transient amplifying cells (TACs) or doublecortin$^+$ (Dcx) neuroblasts. (A) Sample confocal images of coronal sections stained against EDU (red), Sox2 (blue) and GFP (green) from control and inducible conditional knockout (icKO) adult mice. Scale bar, 20 μm. Images are maximum intensity projections of 20 μm 3D stacks. (B) Quantification of Sox2$^+$GFP$^+$ and Sox2$^+$EDU$^+$GFP$^+$ cells compared to the total number of GFP$^+$ cells in control and icKO animals. Each dot represents the mean counts from 3 coronal sections per animal. Bar values represent the mean ± s.e.m. (n = 4 animals per condition for Sox2 quantification and n = 3 animals per condition for Sox2/EDU quantification. *p < 0.05; ***p < 0.001; NS: p > 0.05; one-way ANOVA followed by Sidak's multiple comparisons test). (C) Sample confocal single plane images of Mash1 immunostaining in control and icKO animals. Mash1 immunostaining (red) localizes to the nuclei labeled with DAPI staining (blue). GFP (green) labels the cell membrane. Scale bar, 10 μm. (D) Sample confocal images of Dcx (red) localized to the GFP$^+$ (green) cell bodies in control and icKO animals. Scale bar, 10 μm. (E) Left, quantification of the proportion of Mash1$^+$GFP$^+$ cells compared to the total GFP$^+$ cells in control and icKO animals (n = 6 control and 8 icKO animals. p = 0.57, unpaired t-test). Right, quantification of the proportion of DCX$^+$GFP$^+$ cells compared to the total

GFP$^+$ cells in control and icKO animals (n = 7 control and n = 8 icKO animals. p = 0.53, unpaired t-test).

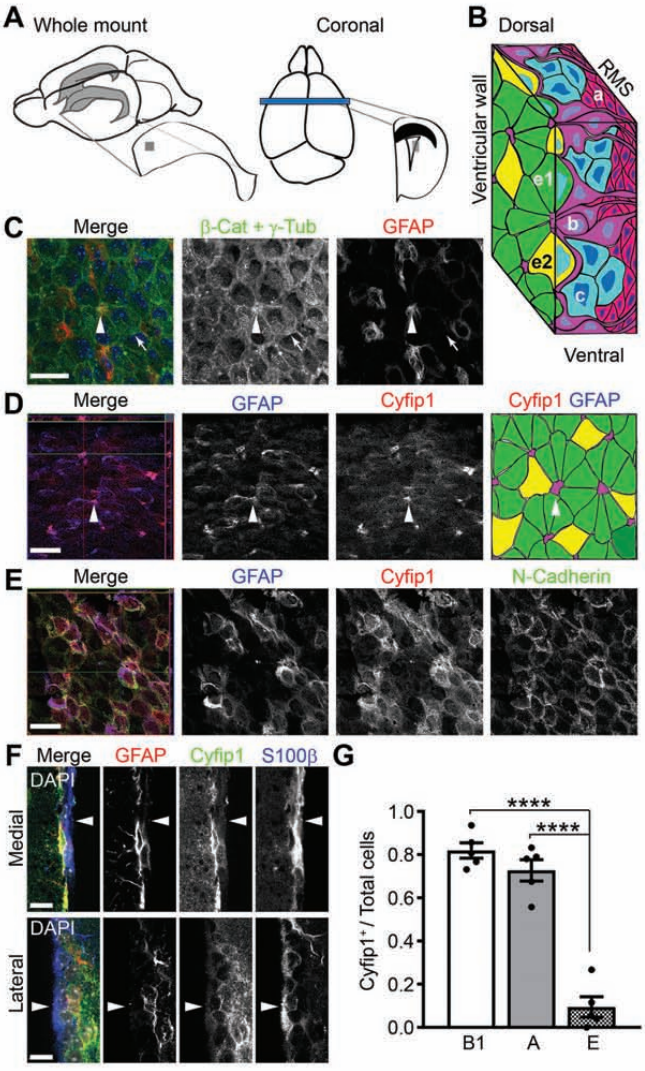

Figure 1 (Habela et al.)

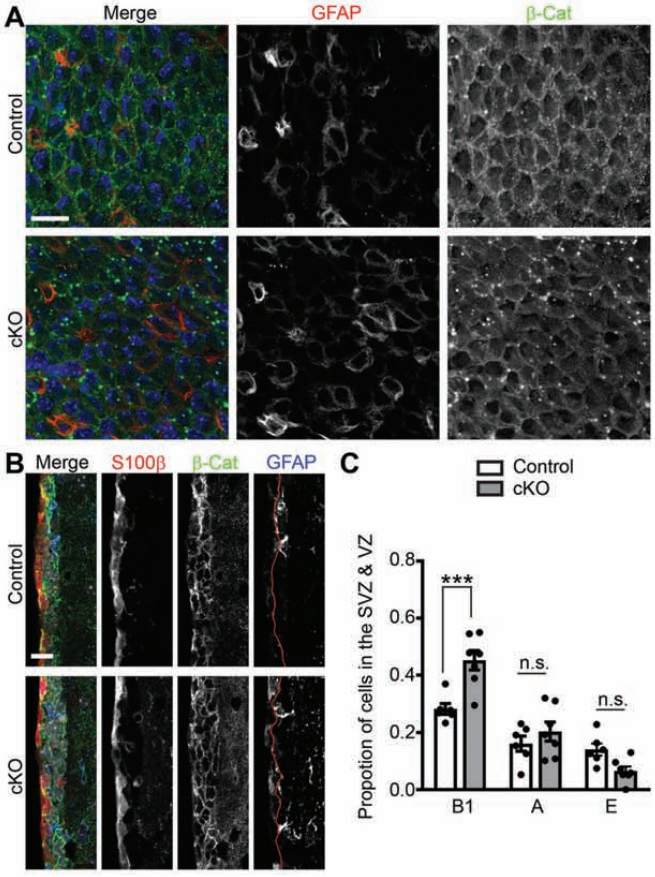

Figure 2 (Habela et al.)

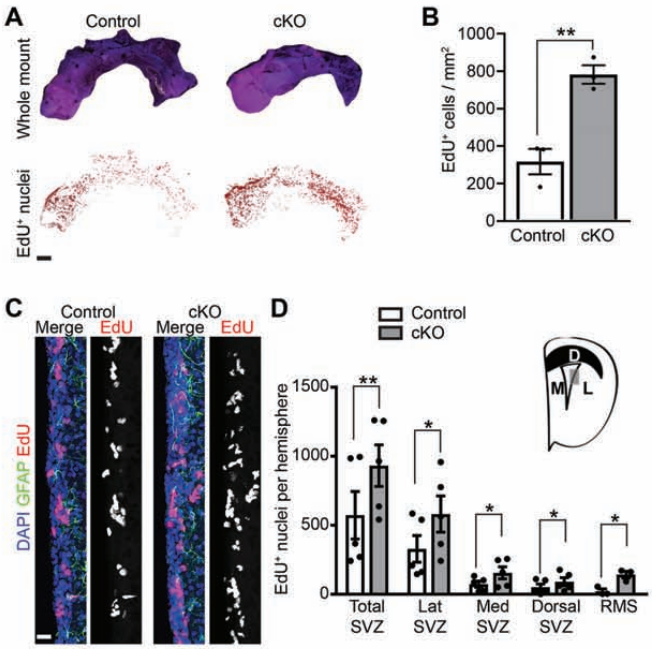

Figure 3 (Habela et al.)

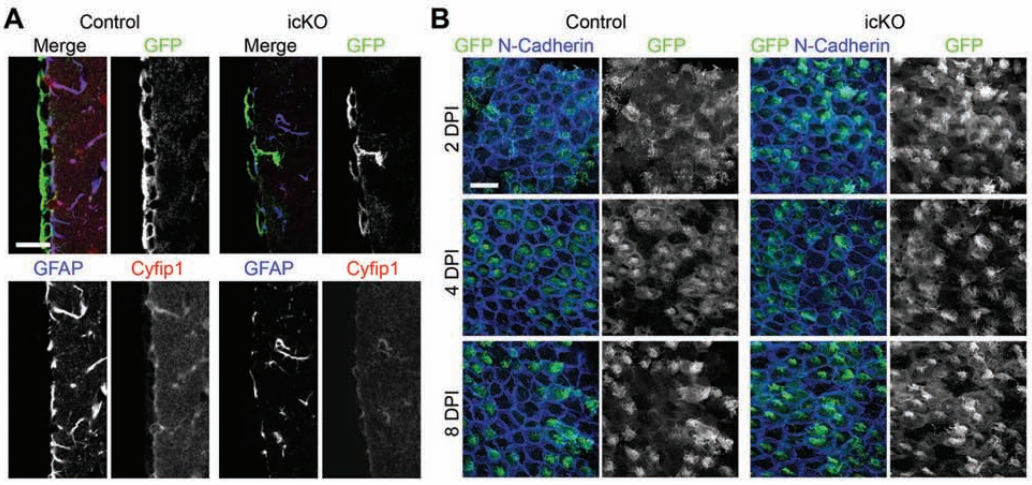

Figure 4 (Habela et al.)

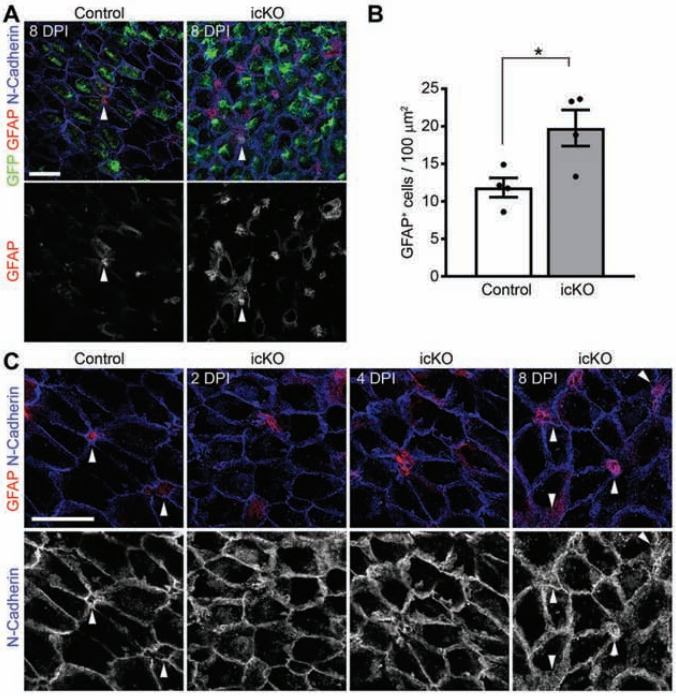

Figure 5 (Habela et al.)

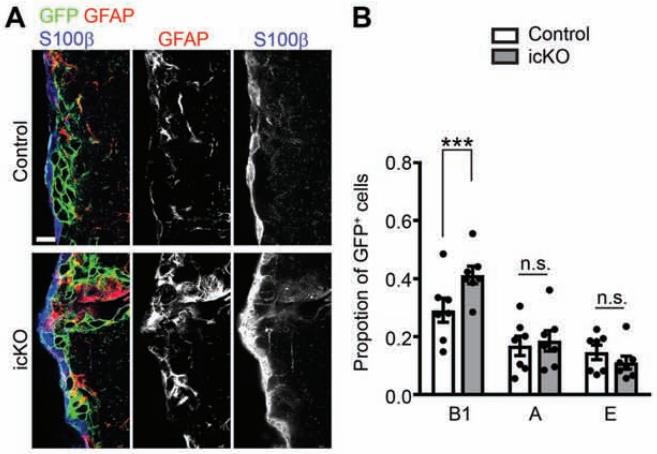

Figure 6 (Habela et al.)

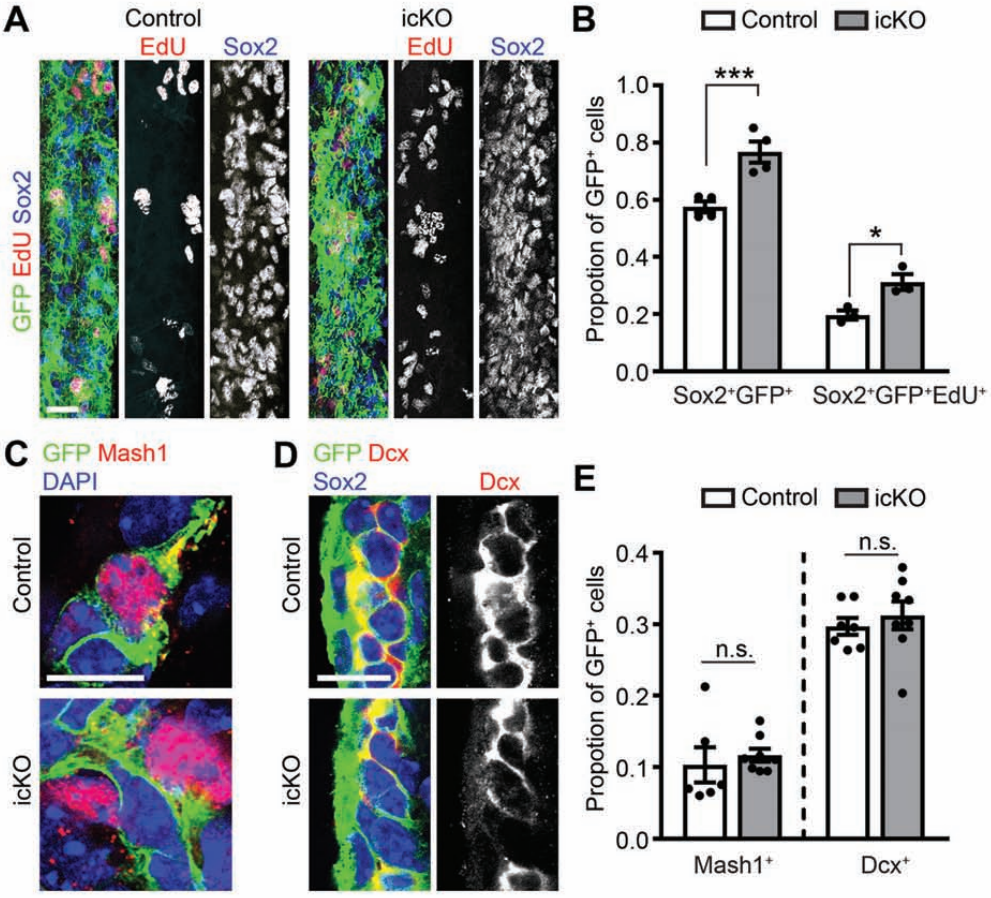

Figure 7 (Habela et al.)